Critical Behavior of Alternately Pumped Nuclear Spins in Quantum Dots

Y. Kondo,[1,2] S. Amaha,[1] K. Ono,[1,3,*] K. Kono,[1,3] and S. Tarucha[1,2]
[1]Center of Emergent Matter Science, RIKEN, 2-1 Hirosawa, Wako, Saitama 351-0198, Japan
[2]Department of Applied Physics, The University of Tokyo, 7-3-1 Hongo, Bunkyo-ku, Tokyo 113-8656, Japan
[3]Low Temperature Physics Laboratory, RIKEN, 2-1 Hirosawa, Wako, Saitama 351-0198, Japan
(Received 12 March 2015; revised manuscript received 3 July 2015; published 27 October 2015)

Nuclear spins in a spin-blocked quantum dot can be pumped and eventually polarized in either of two opposite directions that are selected by applying two different source-drain voltages. Applying a square pulse train as the source-drain voltage can continuously switch the pumping direction alternately. We propose and demonstrate a critical behavior in the polarization after alternate pumping, where the final polarization is sensitive to the initial polarization and pulse conditions. This sensitivity leads to stochastic behavior in the final polarization under nominally the same pumping conditions.

DOI: 10.1103/PhysRevLett.115.186803 PACS numbers: 73.23.Hk, 73.63.Kv, 75.78.-n

Hyperfine interactions between electron spins and nuclear spins are known to produce a variety of phenomena in quantum dots, such as oscillatory behavior, telegraph switching, and hysteresis of the transport current [1–6]. Similar behaviors have also been observed in optically probed quantum dots [7–14]. All these effects were attributed to the nonlinear dynamics of hyperfine-induced dynamical nuclear polarization and its feedback to the electron spin Zeeman energy via the effective nuclear field B_N. The complex interplay between nuclear polarization and electron transport in spin-blocked double quantum dots (DQDs) has been studied theoretically [15–21]. In quantum dots, the existence of a large number of nuclear spins and the hyperfine interaction with electron spins can be a useful resource if they are appropriately manipulated [14,22–26]. Nonlinear dynamics, including chaotic behavior, has attracted long-term interest. The so-called return map is a powerful tool for easily understanding discrete time dynamics [27]. Such dynamics can now be applied to engineering to predict, control, and calculate various complex systems spanning large areas [28].

In this Letter, at first we show a simple return map model describing the interaction between nuclear and electron spin in our system. Then we report a novel characteristic of the nonlinear dynamics of nuclear polarization, a critical behavior of considerably different final states being obtained from slightly different initial states. Nuclear spins in a spin-blocked DQD can be pumped and eventually polarized in either of two opposite directions that are selected by applying two different source-drain voltages V_{SD}. We show that the dynamics of nuclear spins under this alternate pumping exhibits extreme sensitivity to the initial polarization as well as the pumping conditions. Such behavior can be understood by a simple discrete dynamics approximation and so-called return maps. We experimentally demonstrate the critical behavior of the final nuclear polarization after alternate pumping.

A schematic energy diagram of the two-electron energy for a DQD is shown as a function of V_{SD} in Fig. 1(a). The V_{SD}-independent spin triplet states T_+, T_0, and T_- are separated from each other by the effective Zeeman energy $g\mu_B(B_{ext} + B_N)$, where g is the g factor of the electron, μ_B is the Bohr magnetron, and B_{ext} is the external magnetic field. Two spin singlet states, $S(1,1)$ and $S(0,2)$, hybridize and anticross with splitting, reflecting the interdot tunnel

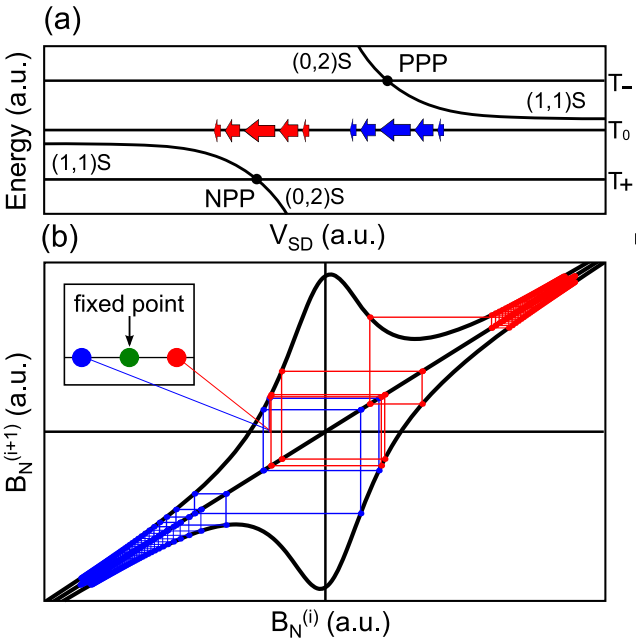

FIG. 1 (color online). (a) Schematic energy diagram of two-electron energy for a DQD as a function of source-drain voltage V_{SD}. The two crossing points, NPP and PPP, and the directions of the shift upon nuclear spin pumping, are indicated by arrows. The lengths of the arrows indicate the strength of pumping at each position. (b) Trajectories of the return map for alternate pumping. The two trajectories start from two initial states that are located very close to the repulsive fixed point.

coupling. The spin blockade loads the electrons to one of the triplet states [29]. Hyperfine-induced elastic flip-flop scattering between an electron spin and a nuclear spin is possible at the two crossing points. At the T_+-S crossing, the accumulation of flopped nuclear spins leads to negative polarization, a decrease in effective Zeeman splitting, and a shift of the crossing point toward a negative V_{SD}. We refer to this crossing point as a negative pumping point (NPP). At the T_--S crossing, positive pumping occurs in a similar manner, causing a shift of the positive pumping point (PPP). These dynamics have been described by the rate equation [15].

The rate equation can be approximated by simpler discrete time dynamics using return maps [27]. For the case of fixed V_{SD} around the NPP, the discrete dynamics of the $(i+1)$th step of B_N, $B_N^{(i+1)}$, is determined from $B_N^{(i+1)} = B_N^{(i)} + f(B_N^{(i)})$ with the Lorentzian function $f(x)$ describing the V_{SD}-dependent pumping strength. For alternate pumping, the return map is $B_N^{(i+1)} = B_N^{(i)} + (-1)^i f(B_N^{(i)})$ [30]. Now the sign of the Lorentzian peak changes with the parity of the pulse number i. This return map can be visually understood in terms of the trajectory, as shown in Fig. 1(b). The rules for the trajectory are as follows. (i) Choose the initial $B_N^{(0)}$ that reflects the detuning of the low or high voltage of the pulse from the NPP or PPP, respectively, under the initial nuclear condition. (ii) Move upward until the inclined Lorentzian having the positive peak is reached. (iii) Move to the right until the inclined straight line is reached. (iv) Move downward until the inclined Lorentzian having the negative peak is reached. (v) Move to the left until the inclined straight line is reached, then go back to (ii).

In Fig. 1(b), the two Lorentzian curves show the up and down pumping curves and the inclined straight line shows the line of symmetry of the two Lorentzian curves. Also, the two trajectories represent the evolutions of $B_N^{(i)}$ from two slightly different initial states near a fixed point where $B_N^{(i+2)} = B_N^{(i)}$. Their final states are considerably different even though the initial states are nearly the same. This critical behavior is due to the repulsive nature of this fixed point. The trajectories that start near the fixed point repeatedly move back and forth around the origin of Fig. 1(b) and eventually move to the left or right. The final state is determined by whether the initial value is larger or smaller than the fixed point. $B_N^{(i)}$ can undergo a huge number of oscillations around the origin before escaping to the left or right, and it appears to be difficult to predict the final state from only the initial behavior. Note that the fixed point changes with the pumping conditions such as the height and width of the Lorentzian. Thus, the final state also shows extreme sensitivity to a slight change in the pumping conditions as well as the initial state.

To experimentally explore the critical behavior of nuclear spins, we measured the transport characteristics of a vertical DQD. The device comprises a submicron pillar structure that consists of an InGaAs quantum well, a GaAs quantum well, and three AlGaAs barriers [31]. The device has two gate electrodes biased with gate voltages V_{G1} and V_{G2}, which enable the control of interdot detuning [4]. Measurements are performed at 1.6 K. The external magnetic field B_{ext} is applied in an in-plane direction. Figure 2(a) shows the differential conductance $dI_{\mathrm{SD}}/dV_{\mathrm{SD}}$ as a function of V_{SD} and the gate voltages at $B_{\mathrm{ext}} = 3.0$ T. The two gate voltages are changed so that interdot detuning remains nearly constant for a fixed V_{SD}. The spin blockade region is observed on the positive-V_{SD} side of the Coulomb diamond for the total electron number $N = 2$. Two lines of the current peak due to the NPP and PPP can be seen, as indicated by the arrows [4].

We next describe the method used to quantitatively measure the effect of alternate pumping. The sequence of V_{SD} used for the alternate pumping is shown in Fig. 2(b), and consists of (1) initialization, (2) alternate pumping, and (3) detection. The measured V_{SD} value can be converted into a B_N value using the experimentally obtained relationship between V_{SD} and B_N [30]. We apply square wave pulse trains with a low voltage V_{SD}^L and a high voltage V_{SD}^H at the same gate voltage, where V_{SD}^L and V_{SD}^H are set to approximately the NPP and PPP, respectively. The frequency and duty ratio of each pulse are 10 MHz and 50%, respectively, unless specifically noted. The total burst time is 1 s, which is much shorter than the relaxation time of nuclear polarization of about 32 s [30]. We prepare the same initial states and discuss the sensitivity to the pumping conditions of the square pulse train.

The lowest trace in Fig. 3(a) is a plot of the change in the nuclear field ΔB_N from its initial value -0.6 T after alternate pumping. Here, we use a square wave pulse train with V_{SD}^L fixed at -0.5 mV, which is much smaller than the

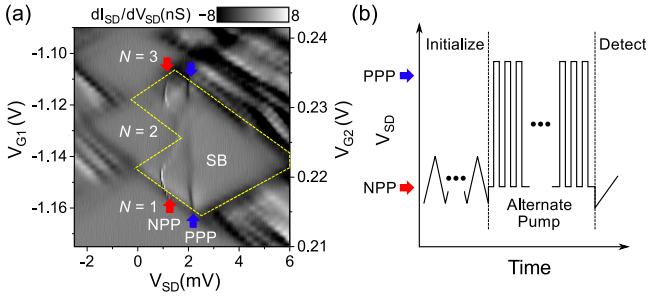

FIG. 2 (color online). (a) Plot of differential conductance $dI_{\mathrm{SD}}/dV_{\mathrm{SD}}$ at $B_{\mathrm{ext}} = 3.0$ T. The two gate voltages V_{G1} and V_{G2} change simultaneously, as shown on the left and right axes, respectively. The spin blockade region is indicated by dashed lines. Arrows indicate the lines of current peaks due to the NPP and PPP. (b) V_{SD} sequence used for alternate pumping measurement.

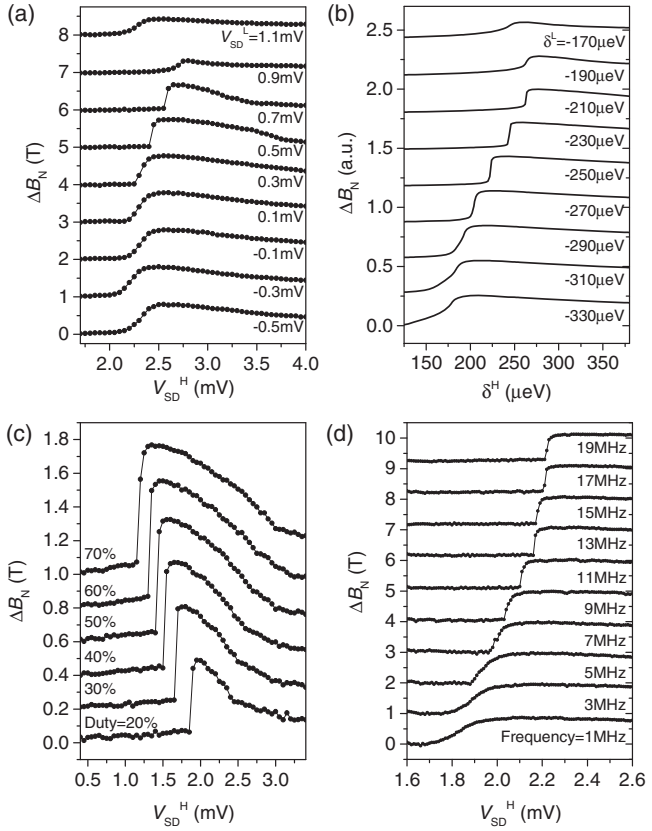

FIG. 3. (a) Plot of the change in the nuclear field ΔB_N after alternate pumping as a function of the high voltage of the square wave pulse train V_{SD}^H at $B_{\mathrm{ext}} = 3.0$ T. Each trace is obtained for a fixed low voltage V_{SD}^L. The traces are offset for clarity. (b) Result of calculation using the rate equation. The horizontal axis is the high value δ^H of the interdot detuning pulse train. Each trace is calculated for different low values δ^L of the pulse train [32]. (c) Duty ratio dependence on V_{SD}^H with V_{SD}^L set at the NPP at $B_{\mathrm{ext}} = 3.0$ T. (d) Dependence of the frequency of the square pulse train on V_{SD}^H with V_{SD}^L set at the NPP.

NPP, and we vary V_{SD}^H. At approximately $V_{\mathrm{SD}}^H = 2.3$ mV, ΔB_N gradually changes from zero to 0.6 T, indicating that V_{SD}^H reaches the PPP and positive pumping occurs. Note that the negative pumping should be sufficiently smaller than the positive pumping under this condition because V_{SD}^L is set away from the NPP. The upper traces show the results of similar measurements with V_{SD}^L changed from −0.3 mV to 1.1 mV. As shown by the trace for $V_{\mathrm{SD}}^L = 0.5$ mV, which is close to the NPP, the transition occurs in a narrower range of V_{SD}^H, indicating the transition of the two final states, a negatively pumped and saturated state, and a positively pumped and saturated state. The transition becomes broader again upon further increase of V_{SD}^L. These behaviors are well reproduced by the rate equation with alternate pumping, as shown in the right panel of Fig. 3(b) [32].

Figure 3(c) shows the results of similar measurements for various duty ratios (ratio of the high voltage to the low voltage). Measurements were performed where V_{SD}^L coincided with the NPP. A sharp transition was observed for all duty ratios, which was accompanied by a shift of the critical V_{SD}^H. The direction of this shift is consistent with the balance between positive and negative pumping. In the discrete dynamic picture, a change in the duty ratio corresponds to different peak heights of the two Lorentzians.

We also repeat similar measurements with various frequencies and burst times of the pulse train. For lower frequencies or shorter burst times, the transition becomes broader for all combinations of V_{SD}^L and V_{SD}^H. This is consistent with the rate equation and the discrete dynamic model. In the return map picture, this is described as a decrease in the repulsive force from the fixed point, resulting in more steps required to reach the final state. For the burst time of 1 s, the sharp transition appears at approximately 10 MHz and remains up to 19 MHz [Fig. 3(d)]. Note that Figs. 3(a), 3(b), and 3(d) were obtained under similar conditions but slightly different gate voltages and interdot detuning, and the values for the critical V_{SD}^H are different in each case.

Systematic statistical measurements were performed for values of V_{SD}^L and V_{SD}^H close to the transition. We repeated the measurement 100 times with nominally the same pulse train to obtain the distribution of the final values of B_N. The initial state was carefully set by scanning V_{SD} 10 times around the NPP. As shown in Fig. 4(a), the observed B_N stochastically takes two different values, −0.4 T and +0.1 T. The three panels correspond to slightly different values for V_{SD}^H around the PPP with the same V_{SD}^L. When $V_{\mathrm{SD}}^H = 2.31$ mV, stochastic behavior with nearly 50% switching probability is observed. We also confirmed that the split distribution is obtained from the simple model calculation used for the return map in Fig. 1(b) [30]. Figure 4(b) is an intensity plot of the distribution for the final B_N as a function of V_{SD}^H for a small range of values around the critical point. The switching probability as a function of V_{SD}^H is plotted in Fig. 4(c). The characteristic transient width is 30 μV. In a GaAs quantum dot containing $\sim 10^5$ nuclear spins, the width of the Gaussian distribution is ∼10 mT. If the stochastic behavior only originates from this state distribution, the transient width will be 0.2 μeV, which is 1 order of magnitude smaller than the observed width. Thus, the observed stochastic behavior originates from the reasonable amount of noise in V_{SD}.

Although the dynamics of nuclear polarization is treated classically in our model, nuclear spin systems are known to behave as quantum systems [33,34]. Indeed, a long coherence time of up to 1 ms was observed for nuclear polarization in the device used in this study [4]. This time scale is 3 orders of magnitude longer than the minimum period of the alternate pumping used in this study. There is little knowledge about the relationship between this quantum nature and nonlinear or chaotic behaviors. The system used in this study is expected to open up new fields in quantum physics and nonlinear or chaos engineering.

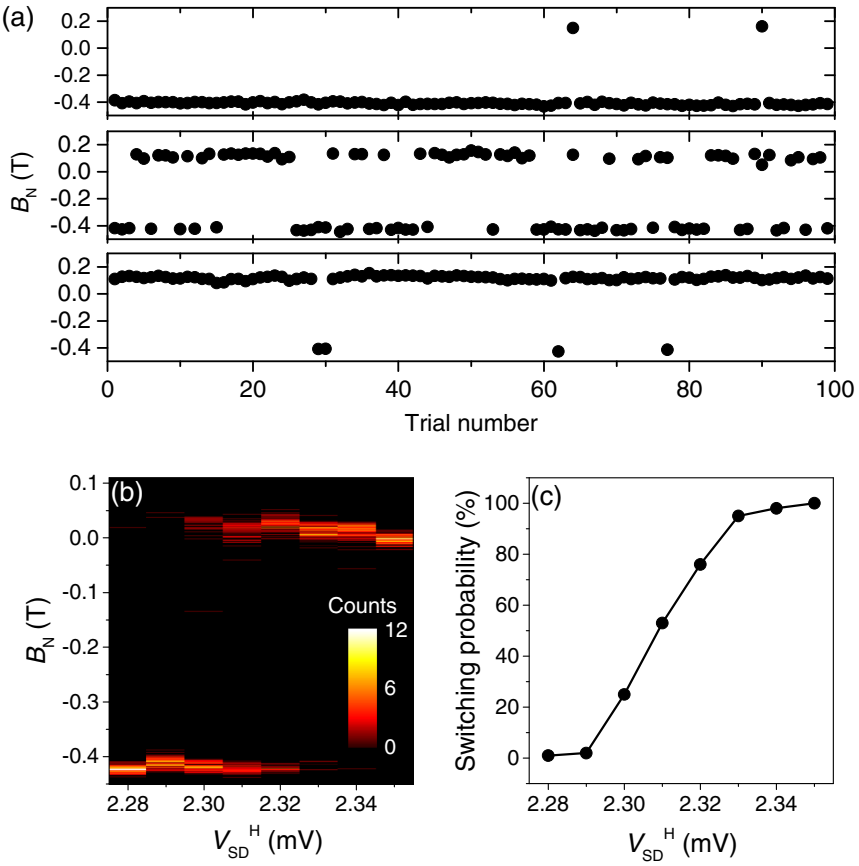

FIG. 4 (color online). (a) Results for B_N in 100 trials under nominally the same alternate pumping conditions for $V_{SD}^H = 2.29$ mV (top), 2.31 mV (middle), and 2.33 mV (bottom) with the same V_{SD}^L of 0.49 mV at $B_{ext} = 3.0$ T. (b) Intensity plot of the count of B_N as a function of V_{SD}^H. (c) Switching probability as a function of V_{SD}^H.

We proposed and demonstrated the critical behavior in alternately pumped nuclear spins in a DQD. The current peak observed in the leakage current of a spin blockade was used to detect the NPP. Nuclear relaxation measurements enabled the quantitative measurement of B_N. After alternate pumping under appropriate conditions, the final value of B_N revealed a transition that is extremely sensitive to the conditions used for positive and negative pumping. This behavior can be understood in terms of the discrete dynamics based on return maps as well as a simulation based on rate equations.

Note that the alternate pumping has various advantages in terms of controllability over more simple unidirectional pumping with relaxation used in previous studies [3,9,10]. In the alternate pumping, the critical behavior is controlled via not only the pumping strength and magnetic field but also the duty ratio and/or frequency of the square wave pulse train. Furthermore, a numerical simulation with different parameters showed that various characteristic behaviors for nonlinear systems, such as a single (and/or) multistable state, semiperiodic and periodic oscillation, and chaotic behavior can appear in the case of more realistic parameters than those in unidirectional pumping [30].

We thank M. Kawamura, G. Kuroda, G. Kurosawa, H. Ando, M. Aono, and K. Aihara for helpful discussions. This work was supported by JSPS KAKENHI Grant No. 11004535 and No. 11J09420.

*k-ono@riken.jp

[1] K. Ono and S. Tarucha, Phys. Rev. Lett. **92**, 256803 (2004).
[2] F. H. L. Koppens *et al.*, Science **309**, 1346 (2005).
[3] J. Baugh, Y. Kitamura, K. Ono, and S. Tarucha, Phys. Rev. Lett. **99**, 096804 (2007).
[4] R. Takahashi, K. Kono, S. Tarucha, and K. Ono, Phys. Rev. Lett. **107**, 026602 (2011).
[5] T. Kobayashi, K. Hitachi, S. Sasaki, and K. Muraki, Phys. Rev. Lett. **107**, 216802 (2011).
[6] E. A. Chekhovich, M. N. Makhonin, A. I. Tartakovskii, A. Yacoby, H. Bluhm, K. C. Nowack, and L. M. K. Vandersypen, Nat. Mater. **12**, 494 (2013).
[7] P.-F. Braun , B. Urbaszek, T. Amand, X. Marie, O. Krebs, B. Eble, A. Lemaitre, and P. Voisin, Phys. Rev. B **74**, 245306 (2006).
[8] M. H. Mikkelsen, J. Berezovsky, N. G. Stoltz, L. A. Coldren, and D. D. Awschalom, Nat. Phys. **3**, 770 (2007).

[9] A. Russell, V. I. Falko, A. I. Tartakovskii, and M. S. Skolnick, Phys. Rev. B **76**, 195310 (2007).
[10] M. N. Makhonin *et al.*, Phys. Rev. B **77**, 125307 (2008).
[11] X. Xu, W. Yao, B. Sun, D. G. Steel, A. S. Bracker, D. Gammon, and L. J. Sham, Nature (London) **459**, 1105 (2009).
[12] C. Latta *et al.*, Nat. Phys. **5**, 758 (2009).
[13] M. N. Makhonin, K. V. Kavokin, P. Senellart, A. Lemaître, A. J. Ramsay, M. S. Skolnick, and A. I. Tartakovskii, Nat. Mater. **10**, 844 (2011).
[14] D. Press, K. De Greve, P. L. McMahon, T. D. Ladd, B. Friess, C. Schneider, M. Kamp, S. Höfling, A. Forchel, and Y. Yamamoto, Nat. Photonics **4**, 367 (2010).
[15] M. S. Rudner and L. S. Levitov, Phys. Rev. Lett. **99**, 036602 (2007).
[16] M. S. Rudner and L. S. Levitov, Phys. Rev. B **82**, 155418 (2010).
[17] J. Danon, I. T. Vink, F. H. L. Koppens, K. C. Nowack, L. M. K. Vandersypen, and Y. V. Nazarov, Phys. Rev. Lett. **103**, 046601 (2009).
[18] M. S. Rudner, I. Neder, L. S. Levitov, and B. I. Halperin, Phys. Rev. B **82**, 041311(R) (2010).
[19] J. Danon and Y. V. Nazarov, Phys. Rev. B **83**, 245306 (2011).
[20] C. Lopez-Monis, C. Emary, G. Kiesslich, G. Platero, and T. Brandes, Phys. Rev. B **85**, 045301 (2012).
[21] M. S. Rudner and L. S. Levitov, Phys. Rev. Lett. **110**, 086601 (2013).
[22] A. V. Khaetskii, D. Loss, and L. Glazman, Phys. Rev. Lett. **88**, 186802 (2002).
[23] I. A. Merkulov, A. L. Efros, and M. Rosen, Phys. Rev. B **65**, 205309 (2002).
[24] J. R. Petta *et al.*, Science **309**, 2180 (2005).
[25] F. H. L. Koppens, K. C. Nowack, and L. M. K. Vandersypen, Phys. Rev. Lett. **100**, 236802 (2008).
[26] H. Bluhm, S. Foletti, D. Mahalu, V. Umansky, and A. Yacoby, Phys. Rev. Lett. **105**, 216803 (2010).
[27] R. M. May, Nature (London) **261**, 459 (1976).
[28] K. Aihara, Proc. IEEE **90**, 919 (2002).
[29] K. Ono, D. G. Austing, Y. Tokura, and S. Tarucha, Science **297**, 1313 (2002).
[30] See Supplemental Material at http://link.aps.org/supplemental/10.1103/PhysRevLett.115.186803 for details of the measurement method and the calculation result using return map model shown in main text.
[31] S. M. Huang, Y. Tokura, H. Akimoto, K. Kono, J. J. Lin, S. Tarucha, and K. Ono, Phys. Rev. Lett. **104**, 136801 (2010).
[32] Calculations were performed on the basis of Ref. [15]. The parameters used were $t = 160\ \mu$eV, $\tau = 1\ \mu$eV, $\tau_0^{-1} = 200$ MHz, $g = -0.44$, $B = 3.0$ T, $N = 10^5$, $\alpha N = -5$ T, $B_N^{\text{initial}} = -0.12N$, and $\Gamma_{\text{rel}} = 0.0005\ \text{s}^{-1}$. The same symbols as those in Ref. [15] were used. The square wave pulse with various low or high detuning δ^L or δ^H, shown in Fig. 3(b) with a frequency of 10 MHz and a burst time of 0.5 ms, was used. Note that we used rather strong pumping parameters and a shorter burst time to obtain a result within a reasonable calculation time.
[33] Y. Kondo, M. Ono, S. Matsuzaka, K. Morita, H. Sanada, Y. Ohno, and H. Ohno, Phys. Rev. Lett. **101**, 207601 (2008).
[34] G. Yusa, K. Muraki, K. Takashina, K. Hashimoto, and Y. Hirayama, Nature (London) **434**, 1001 (2005).